

# Journal of Materials Chemistry C

Accepted Manuscript



This is an *Accepted Manuscript*, which has been through the Royal Society of Chemistry peer review process and has been accepted for publication.

*Accepted Manuscripts* are published online shortly after acceptance, before technical editing, formatting and proof reading. Using this free service, authors can make their results available to the community, in citable form, before we publish the edited article. We will replace this *Accepted Manuscript* with the edited and formatted *Advance Article* as soon as it is available.

You can find more information about *Accepted Manuscripts* in the [Information for Authors](#).

Please note that technical editing may introduce minor changes to the text and/or graphics, which may alter content. The journal's standard [Terms & Conditions](#) and the [Ethical guidelines](#) still apply. In no event shall the Royal Society of Chemistry be held responsible for any errors or omissions in this *Accepted Manuscript* or any consequences arising from the use of any information it contains.

## Photovoltaic properties of bis(octyloxy)benzo-[c][1,2,5]thiadiazole sensitizers based on *N,N*-diphenylthiophen-2-amine donor

Cite this: DOI: 10.1039/x0xx00000x

Received 00th January 2012,  
Accepted 00th January 2012

DOI: 10.1039/x0xx00000x

www.rsc.org/

Xiaoyu Zhang,<sup>a</sup> Long Chen,<sup>a</sup> Xin Li,<sup>b</sup> Jiangyi Mao,<sup>a</sup> Wenjun Wu,<sup>a</sup> Hans Ågren,<sup>b</sup> and Jianli Hua<sup>a\*</sup>

In this paper, we have designed and synthesized three D-A- $\pi$ -A sensitizers (**DOBT-IV~VI**) with *N,N*-diphenylthiophen-2-amine as donor and bis(octyloxy)benzo-[c][1,2,5]thiadiazole (DOBT) as the auxiliary acceptor. Their applications to dye-sensitized solar cells with I<sup>-</sup>/I<sub>3</sub><sup>-</sup> and Co(II)/(III) electrolyte were measured and characterized. Via fine tuning of the  $\pi$ -bridge, we obtained the highest photoelectric conversion efficiency of 7.16 % with  $J_{sc} = 16.88 \text{ mAcm}^{-2}$ ,  $V_{oc} = 0.662 \text{ V}$  and FF = 64.03% for the **DOBT-V**-based DSSCs employing iodide/triiodide electrolyte and of 6.14% for cobalt electrolyte with  $J_{sc} = 11.35 \text{ mAcm}^{-2}$ ,  $V_{oc} = 0.760 \text{ V}$  and FF = 71.16% under standard global AM1.5 solar conditions. Density functional theory calculations, behaviour study of the four performance parameters with dependence of incident light intensity, electrochemical impedance spectroscopy and intensity-modulated photovoltage spectroscopy were employed to evaluate and investigate their optical and electrochemical properties and photovoltaic performance.

### Introduction

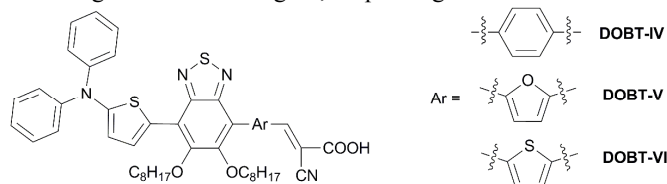
As entering the twenty-first century, the world is suffering from many serious issues, one of which is energy crisis. A worldwide research and development of renewable energy have been booming. In just two decades, we have witnessed the birth of dye-sensitized solar cells (DSSCs)<sup>1</sup> and its flourish. Till now, the world record have been kept above 15% by perovskite-based DSSCs.<sup>2</sup> For organic sensitizer, the overall photoelectric conversion efficiency of 13.0% has been reached by using zincporphyrin-based sensitizer and cobalt-based electrolyte without using co-sensitization.<sup>3</sup> In order to achieve higher photoelectric conversion efficiency, the short-circuit current density ( $J_{sc}$ ) and the open-circuit voltage ( $V_{oc}$ ) should be improved. There are many strategies having been put forward to attain high efficiencies.<sup>4</sup>

The electrolyte, which plays a significant role on DSSCs' photovoltaic performance, has attracted tremendous attention from all over the world. The traditional electrolyte, known as iodide/triiodide electrolyte, is suffering from problems such as competitive light absorption with sensitizers and the corrosiveness towards most metals and sealing materials. To solve these problems, cobalt complexes emerged as an alternative of iodide/triiodide.<sup>5</sup> Owing to their tuneable and more positive redox potentials, they soon became a star among all the redox couples. High open-circuit voltages usually can be achieved via Co(II)/(III) electrolyte-based DSSC devices. However, due to their larger size, heavier mass and slower diffusion in electrolyte, their mass transport is limited and charge recombination is severe. In order to retard the

recombination, bulky sensitizers are chosen to work with Co(II)/(III) electrolyte.<sup>6</sup>

Another crucial factor is the sensitizer. Pure organic sensitizers have drawn increasing attention for their easy and low-cost accesses of molecular structure design to fine adjust their properties such as molecular geometries, molar extinction coefficients, absorption properties and energy levels, thus to achieve relatively high efficiency.<sup>7</sup> Generally they have the donor- $\pi$  bridge-acceptor (D- $\pi$ -A) configuration with the virtue of intramolecular charge transfer (ICT) property.<sup>8</sup> Recent researches have showed that introducing an additional electron-withdrawing unit between the donor and the  $\pi$ -bridge as auxiliary acceptor can not only tune the molecular energy levels but also red-shift the charge-transfer absorption band, leading to the improvement of photovoltaic performance and stability.<sup>9</sup> Many auxiliary acceptor units have been adopted successfully, such as benzothiadiazole,<sup>10</sup> benzotriazole,<sup>11</sup> quinoxaline,<sup>12</sup> diketopyrrolo-pyrrole,<sup>13</sup> pyrido[3,4-b]pyrazine,<sup>14</sup> and thieno[3,4-c]pyrrole-4,6-dione.<sup>15</sup>

Among them, benzothiadiazole shows some advantages in light-harvesting and efficiency, including expanding absorption wavelengths into NIR region, improving electron distribution



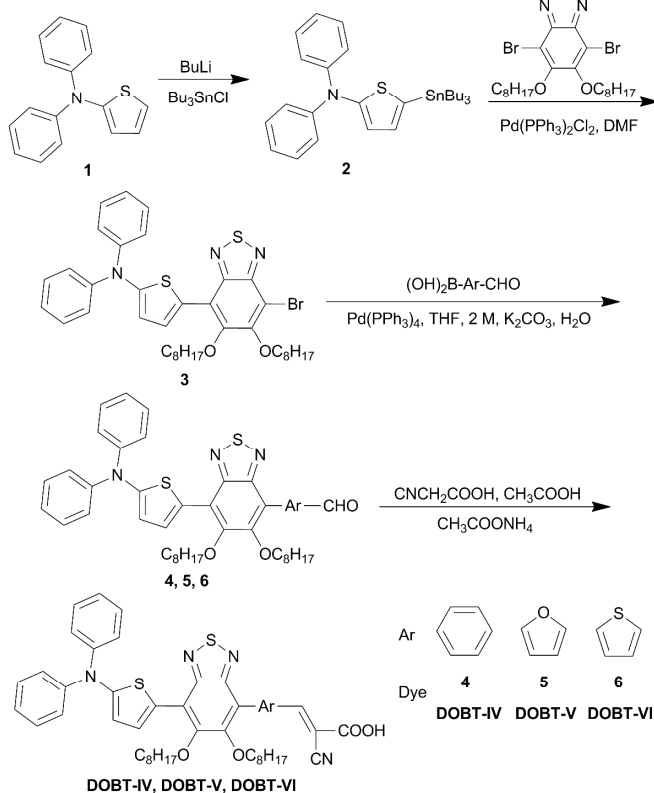
Scheme 1. Molecular structures of the dyes **DOBT-IV~VI**.

and increasing the photo-stability of synthetic intermediates and target sensitizers.<sup>16</sup> However, the low open current voltage ( $V_{oc}$ ) limits its performance in dye-sensitized solar cells.<sup>17</sup> In our previous work, we introduced two longer alkyl chains onto benzothiadiazole units to construct three triarylamine-based sensitizers (**BODT-I-III**).<sup>18</sup> The results exhibited that sensitizers using 5,6-bis(octyloxy)benzo[*c*]-[1,2,5]thiadiazole had higher open-circuit voltages compared with that of a benzothiadiazole-containing analogue.

With the intention of pursuing higher short-circuit current density, we replaced the triphenylamine unit with *N,N*-diphenylthiophen-2-amine unit, which has better electron-donating ability, to further broad the absorption range.<sup>19</sup> Therefore, in this paper, we designed and synthesized three D-A- $\pi$ -A sensitizers, **DOBT-IV-VI** (see **Scheme 1**) with *N,N*-diphenylthiophen-2-amine as donor, DOBT as the auxiliary acceptor, and benzene, thiophene and furan rings adopted to fine tune the properties of the sensitizers. Their photovoltaic performance were also measured and analyzed. In order to enhance the  $V_{oc}$ , we also used cobalt electrolyte in the devices. As expected, the  $V_{oc}$  increased largely, but the  $J_{sc}$  dropped, resulting in a decreased photoelectric conversion efficiency (PCE).

## Synthetic procedures

The synthesis procedures of **DOBT-IV-VI** are depicted in **Scheme 2**. Compound **3** was synthesized via the Suzuki coupling reaction between 4,7-dibromo-5,6-bis(octyloxy)-benzo[*c*]-[1,2,5]thiadiazole and tributyltin compound **2**, which was derived from *N,N*-diphenylthiophen-2-amine. Then (4-formylphenyl)boronic acid, (5-formylfuran-2-yl)boronic acid and (5-formylthiophen-2-yl)boronic acid reacted with compound **3** respectively to obtain the corresponding aldehyde



**Scheme 2.** The synthesis of the dyes **DOBT-IV-VI**.

precursors (compounds **4**, **5**, **6**), followed by Knoevenagel condensation with cyanoacetic acid to produce the target dyes (**DOBT-IV-VI**). All the intermediates and three target sensitizers were fully characterized with <sup>1</sup>H NMR, <sup>13</sup>C NMR and HRMS.

## Results and discussion

### Optical and electrochemical properties

The absorption spectra of the three dyes in the CH<sub>2</sub>Cl<sub>2</sub> solvent and on 4  $\mu$ m transparent TiO<sub>2</sub> films are shown in **Fig. 1**. We can see that, in the CH<sub>2</sub>Cl<sub>2</sub> solvent, both **DOBT-V** and **DOBT-VI** exhibit three major absorption bands appearing at 300-370 nm, 370-450 nm, and 450-700 nm, while **DOBT-IV** only displays two major absorption bands appearing at 300-410 nm and 410-620 nm. It is clear that the introduction of heterocyclic rings results in the emergence of the new absorption band because of the n- $\pi^*$  transitions. The first absorption band can be attributed to  $\pi$ - $\pi^*$  transitions caused by the conjugation of DOBT moiety and the  $\pi$ -bridge, whilst the last absorption band can be assigned to the intramolecular charge transfer (ICT) between the *N,N*-diphenylthiophen-2-amine donor and cyanoacetic acid acceptor moiety. The main absorption peaks of **DOBT-IV**, **DOBT-V** and **DOBT-VI** are at 483 nm, 525 nm and 531 nm, respectively. The 42-48 nm bathochromic shifts of the main absorption peaks of **DOBT-V** and **DOBT-VI** compared to **DOBT-IV** can be ascribed to the much better planarity between DOBT moiety and thiophene or furan moiety compared to that between DOBT and benzene (see **Fig. S2**), which would benefit the intramolecular charge transfer.

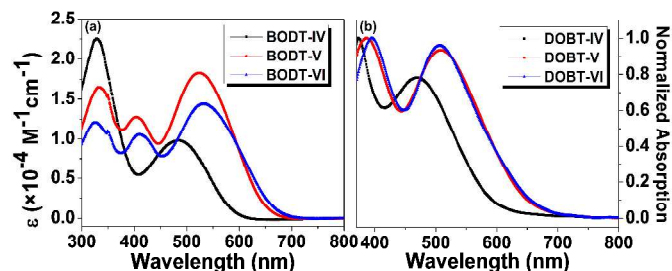


**Fig. 1.** Absorption spectra of **DOBT-IV-VI** in CH<sub>2</sub>Cl<sub>2</sub> (a) and on 4  $\mu$ m transparent TiO<sub>2</sub> films (b).

To estimate the feasibility of the electron injection into the conduction band of TiO<sub>2</sub> and dye regeneration, cyclic voltammetry (CV) measurement was carried out in CH<sub>2</sub>Cl<sub>2</sub> solution with 0.1 M tetra-*n*-butylammonium hexafluorophosphate (TBAPF<sub>6</sub>) as the inert electrolyte with a three-electrode system (working electrode: Pt; counter electrode: Pt wire; reference electrode: SCE; calibrated with ferrocene/ferrocenium (Fc/Fc<sup>+</sup>) as an internal reference). The cyclic voltammograms of **DOBT-IV-VI** are shown in **Fig. S1**. The redox potentials ( $E_{ox}$ ) of **DOBT-IV-VI** are corresponding to the highest occupied molecular orbital (HOMO) energy levels, locating at 0.71, 0.72, and 0.71 V vs. NHE, respectively. The nearly equal HOMO energy levels of **DOBT-IV-VI** indicate that the HOMO energy level mainly depends on the donor moiety. All the parameters of electrochemical properties of **DOBT-IV-VI** are listed in **Table 1**. The zero-zero transition energies ( $E_{0-0}$ ) of **DOBT-IV-VI** are 2.11 eV, 1.90 eV, and 1.92 eV, respectively, which were estimated from the intersection of the normalized absorption and emission spectra via the equation of  $E_{0-0} = 1240/\lambda$ . Calculated from  $E_{HOMO} - E_{0-0}$ , the lowest unoccupied molecular orbital (LUMO) energy levels are -1.40, -1.18, and -1.21 V vs. NHE, respectively. As we all know, to

be a good sensitizer for DSSCs, a dye's LUMO energy level has to be at least 0.20 V higher than the conduction band energy level ( $E_{cb}$ ) of  $TiO_2$  (-0.5 V vs. NHE) to fulfil an efficient injection of the excited electrons into the conduction band, while its HOMO energy level must be at least 0.15 V lower than the redox potential of the electrolyte to guarantee an efficient regeneration of the oxidized dyes by the redox species in the electrolyte.<sup>20</sup> With their LUMO values that are about 0.7-0.9 V more negative than the  $E_{cb}$  of  $TiO_2$  whilst their HOMO values which are 0.3 V more positive than the redox potential of  $I/I_3^-$  (0.4 V vs. NHE) and 0.15 V more positive than the redox potential  $Co(II)/Co(III)$  (0.56 V vs. NHE), **DOBT-IV~VI** are qualified for the application to DSSCs in theory.

**Table 1.** Optical properties and electrochemical properties of the dyes **DOBT-IV~VI**.

Dye	$\lambda_{max}^{[a]}$ /nm ( $\times 10^3 M^{-1} cm^{-1}$ )	$\lambda_{max}^{[b]}$ $TiO_2$ /nm	HOMO <sup>[c]</sup> /V (vs. NHE)	$E_{0-0}$ <sup>[d]</sup> /eV	LUMO <sup>[e]</sup> /V (vs. NHE)
<b>DOBT-IV</b>	483(1.01)	467	0.71	2.11	-1.40
<b>DOBT-V</b>	525(1.82)	508	0.72	1.90	-1.18
<b>DOBT-VI</b>	531(1.34)	506	0.71	1.92	-1.21

<sup>[a]</sup>Absorption maximum in  $CH_2Cl_2$  solution. <sup>[b]</sup>Absorption maximum on  $TiO_2$  film (without CDCA). <sup>[c]</sup>HOMO energy levels were measured in  $CH_2Cl_2$  with 0.1 M tetra-n-butylammonium hexafluorophosphate (TBAPF<sub>6</sub>) as electrolyte (working electrode: Pt; reference electrode: SCE; calibrated with ferrocene/ferrocenium (Fc/Fc<sup>+</sup>)). <sup>[d]</sup> $E_{0-0}$  was estimated from the intercept of the normalized absorption and emission spectra of the dyes.  $E_{0-0} = 1240/\lambda$ . <sup>[e]</sup>LUMO energy levels were estimated by subtracting  $E_{0-0}$  from the HOMO energy level.

### Molecular Orbital Calculations

We employed density functional theory (DFT) calculations to further investigate the intermolecular electron transfer. According to Preat et al.,<sup>21</sup> the free energy change for the electron injection process can be expressed as

$$\Delta G^{inject} = E_{OX}(ES) - E_{CB}(TiO_2)$$

where  $E_{CB}(TiO_2)$  is the reduction potential of the conduction band of  $TiO_2$  (4.0 eV) and  $E_{OX}(ES)$  is the oxidation potential of the dye in the excited state which is equal to the difference between  $E_{OX}(GS)$ , the oxidation potential of the dye in the ground state, and  $\lambda_{max}$ , the excitation energy corresponding to the photoinduced intramolecular charge transfer (ICT) absorption band

$$E_{OX}(ES) = E_{OX}(GS) - \lambda_{max}$$

In this work, the hybrid B3LYP functional<sup>22,23</sup> and the 6-31G\* basis set<sup>23</sup> were adopted in geometry optimizations of organic dyes and calculations of their  $E_{OX}(GS)$  values. For  $\lambda_{max}$ , time-dependent density functional theory (TDDFT) calculations were carried out with the hybrid BHandHLYP functional<sup>22,23,25</sup> and the 6-31G\* basis set,<sup>23</sup> which is a feasible choice for the study of excitations with charge-transfer character. As suggested by Preat et al.,<sup>21</sup> the electron injection process was assumed to occur before the relaxation in excited state, and the nonequilibrium polarizable continuum model (PCM)<sup>26</sup> was selected to model the solvent effects of dichloromethane. All theoretical calculations were carried out using the Gaussian 09 program package.<sup>22</sup>

The computed key parameters of DSSCs are listed in **Table S1**. With the help of theoretical calculations we are able to gain insight into the factors that may influence the performance of DSSC dyes. First, the magnitude of  $E_{OX}(GS)$  is closely related to the energy level of the highest occupied molecular orbital (HOMO) (see **Table S2**), which is mainly localized on the donor part of the organic dye. Therefore the choice of a proper donor group is of great importance in the design of DSSC dyes. It is shown that in **DOBT-IV**, **DOBT-V** and **DOBT-VI** the donor part is almost coplanar with the benzothiadiazole group, leading to a lifted energy level of HOMO and hence a smaller  $E_{OX}(GS)$  which is not benefit for the regeneration of the dye cation radical. Besides, the choice of  $\pi$ -conjugation bridge between DOBT and cyanoacrylic acid also matters. When a phenyl ring is used to connect the benzothiadiazole and

cyanoacrylic acid groups, the energy level of LUMO is lifted, resulting in a larger HOMO-LUMO gap, a larger  $-\Delta G^{inject}$  and a smaller oscillator strength of the ICT absorption band (e.g. **DOBT-IV**) which leads to lower efficiency of light harvesting. When a thiophene or furan ring is employed as  $\pi$ -conjugation bridge, the HOMO-LUMO gap decreases, leading to a diminished  $-\Delta G^{inject}$  and an enhanced oscillator strength. **Fig. 2** shows the dependence of  $-\Delta G^{inject}$  and oscillator strength of ICT absorption band on HOMO-LUMO gap, from which it can be seen that  $-\Delta G^{inject}$  is positively and linearly correlated to HOMO-LUMO gap for **DOBT-IV~VI**. Interestingly, the magnitude of oscillator strength is negatively and linearly correlated to HOMO-LUMO gap. According to our previous work,<sup>27</sup> we brought up with two principles for the design of DSSC dyes: (1) a large  $E_{OX}(GS)$  and (2) the choice of an appropriate  $\pi$ -bridge which ensures a good balance between  $-\Delta G^{inject}$  and the oscillator strength of the ICT absorption band. From **Fig. 2** it is clear that although none of **DOBT-IV~VI** exhibits a good balance between  $-\Delta G^{inject}$  and oscillator strength of the ICT absorption band, **DOBT-V** is slightly better than the other two dyes. From the theoretical analysis, we can predict that **DOBT-VI** might show the worst performance since

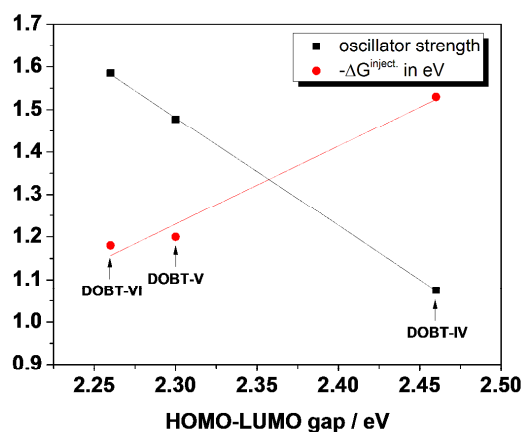


**Fig. 2.** Dependence of  $-\Delta G^{inject}$  and oscillator strength of ICT absorption band on HOMO-LUMO gap.

it has neither a large  $E_{OX}(GS)$  nor a good balance between  $-\Delta G^{inject}$  and the oscillator strength of the ICT absorption band, which has been proved by the results of the DSSCs characterizations.

**Fig. S2** depicts the frontier orbitals of **DOBT-IV~VI**, calculated at (isodensity = 0.020 a.u.) Hydrogens are omitted for clarity. The dihedral angles between the DOBT and donor moiety and the ones between  $\pi$ -bridge are also showed in **Fig. S2**. We can see that the introduction of heterocyclic rings largely reduced the dihedral angle between DOBT and the  $\pi$ -bridge, from 42.7° for benzene as the  $\pi$ -bridge to 10.2° for thiophene moiety and 4.6° for furan moiety, improving the planarity of the molecular structure, which can facilitate the charge transfer, while at the same time may increase the likelihood of dye aggregation and electron recombination.

### Photovoltaic Performance of DSSCs

The DSSCs based on **DOBT-IV~VI** employed two different electrolytes.  $I/I_3^-$ -based electrolyte consisted of 0.05 M  $I_2$ , 0.1 M LiI, 0.5 M 1,2-dimethyl-3-propylimidazolium iodide (DMPiI), 0.75 M 4-tert-butylpyridine (tBP) in acetonitrile, whereas  $Co(II)/(III)$ -based electrolyte was composed of 0.22 M tris(2, 2'-bipyridine)cobalt(II) bis(hexafluorophosphate) ( $[Co(bpy)_3]$  (PF<sub>6</sub>)<sub>2</sub>),

0.05 M tris(2,2'-bipyridine)cobalt(III)tris(hexafluorophosphate)([Co(bpy)<sub>3</sub>](PF<sub>6</sub>)<sub>3</sub>), 0.1 M LiClO<sub>4</sub>, 0.2 M tBP in acetonitrile. Fig. 3 shows the incident photon-to-electron conversion efficiency (IPCE) as a function of incident wavelength for DSSCs based on these dyes with the two electrolytes. Compared the IPCE of DSSCs with iodide/triiodide electrolyte with those in our previous work,<sup>18</sup> the IPCE ranges of the three dyes were enlarged to near-infrared region by replacing the triphenylamine with *N,N*-diphenylthiophen-2-amine unit. What's more, the ranges were further broadened in accordance with the absorption spectrum via substituting the benzene ring with heterocyclic rings, which would benefit the photoinduced current density. However, the IPCE values of DOBT-V are higher than that of DOBT-VI, which might be owing to the high molecular extinction coefficient of DOBT-V (18200 M<sup>-1</sup>cm<sup>-1</sup>) despite their similar planarity of the molecular structure. The IPCE values of DSSCs with Co(II)/(III) electrolyte exhibit the similar trend among the three dyes, but are much lower than that of their counterparts with I<sup>-</sup>/I<sub>3</sub><sup>-</sup> electrolyte, indicating lower short current densities (*J*<sub>sc</sub>). To be more specific, DOBT-IV-sensitized solar cell with I<sup>-</sup>/I<sub>3</sub><sup>-</sup> electrolyte shows the IPCE above 60% at the range of 380-590 nm with the highest value of 72% while the one with Co(II)/(III) electrolyte displays the IPCE above 45% at the range of 360-570 nm

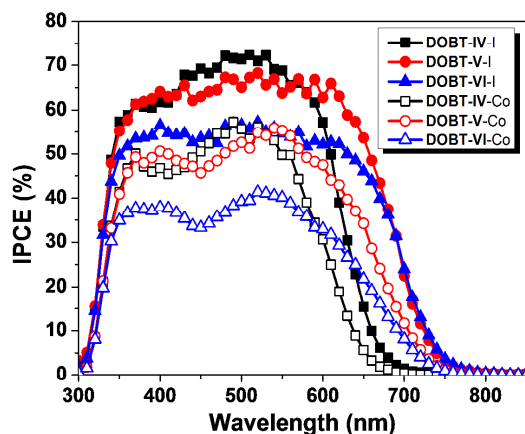


Fig. 3. The IPCE spectra of DOBT-IV~VI-based DSSCs with Co(II)/(III) and I<sup>-</sup>/I<sub>3</sub><sup>-</sup> electrolyte.

with the highest value of 57% at 490 nm. That could explain the big gap *J*<sub>sc</sub> values between the two electrolytes. Similarly, at the range of 370-620 nm, the IPCE values of DOBT-V-sensitized solar cell with I<sup>-</sup>/I<sub>3</sub><sup>-</sup> electrolyte are above 60% whilst that with Co(II)/(III) electrolyte are only above 40% with the highest value of 56%. However, the IPCE for DOBT-VI-sensitized solar cell is quiet low, reaching only over 30% from 340 nm to 620 nm with the highest value of 41% at 540 nm for Co(II)/(III) electrolyte and over 50% from 360 nm to 620 nm with the highest value of 57% for I<sup>-</sup>/I<sub>3</sub><sup>-</sup> electrolyte.

Table 2 shows all the photovoltaic parameters of DSSCs based on DOBT-IV~VI with I<sup>-</sup>/I<sub>3</sub><sup>-</sup> and Co(II)/(III) electrolyte. For DSSCs with I<sup>-</sup>/I<sub>3</sub><sup>-</sup> electrolyte, the *J*<sub>sc</sub> of DOBT-V-based DSSC is higher than that of DOBT-IV- and DOBT-VI-based DSSC. Given its broadened absorption range, enhanced molar extinction coefficient and high IPCE values, there is no wonder DOBT-V exhibits the best performance on the short circuit current. What's more, the DSSCs display the same order of other parameters: *V*<sub>oc</sub> (DOBT-IV) > *V*<sub>oc</sub> (DOBT-V) > *V*<sub>oc</sub> (DOBT-IV). The detailed discussion of the *V*<sub>oc</sub> will be found in the following sections of electrochemical impedance spectroscopy (EIS) and intensity modulated photovoltage

spectroscopy (IMVS). Finally, the highest photovoltaic conversion efficiency (PCE) was obtained by DOBT-V-based DSSCs as 7.16% with *J*<sub>sc</sub> = 16.88 mAcm<sup>-2</sup>, *V*<sub>oc</sub> = 0.662 V and FF = 64.03% for iodide/triiodide electrolyte. The similar changing pattern is found in DSSCs with cobalt electrolyte and their highest photovoltaic conversion efficiency of 6.14% was gained also by DOBT-V-based DSSCs with *J*<sub>sc</sub> = 11.35 mAcm<sup>-2</sup>, *V*<sub>oc</sub> = 0.760 V and FF = 71.16% under standard global AM1.5 solar conditions.

Table 2. Photovoltaic parameters of DSSCs based on DOBT-IV~VI with I<sup>-</sup>/I<sub>3</sub><sup>-</sup> and Co(II)/(III) electrolyte.

Dye	<i>J</i> <sub>sc</sub> (mAcm <sup>-2</sup> )	<i>V</i> <sub>oc</sub> (V)	FF (%)	PCE (%)
DOBT-IV-I	15.05	0.686	64.53	6.66
DOBT-V-I	16.88	0.662	64.03	7.16
DOBT-VI-I	15.37	0.629	64.02	6.19
DOBT-IV-Co	9.96	0.774	73.44	5.66
DOBT-V-Co	11.35	0.760	71.16	6.14
DOBT-VI-Co	8.37	0.713	71.06	4.24

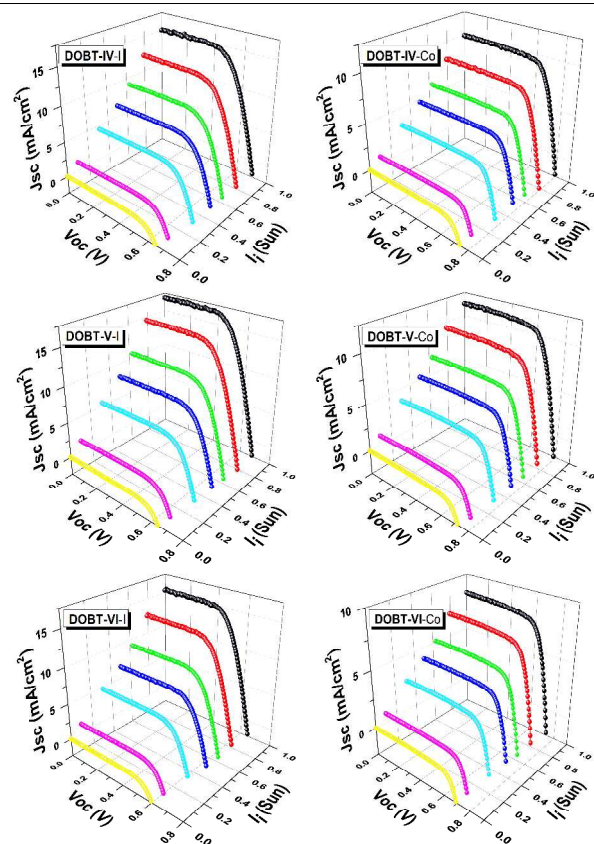
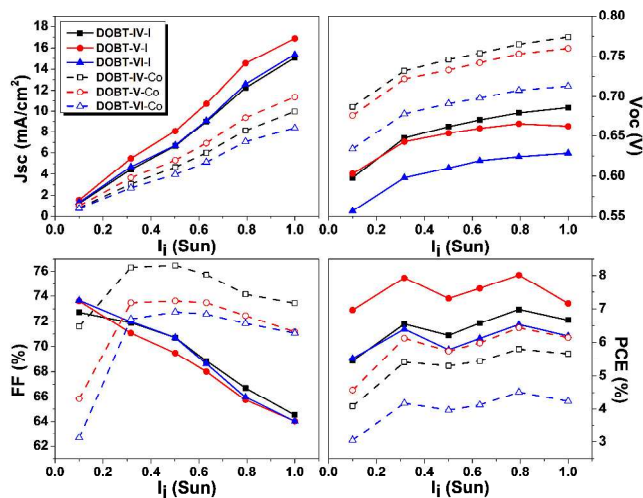


Fig. 4. The I-V curves of DOBT-IV~VI-based DSSCs with Co(II)/(III) and I<sup>-</sup>/I<sub>3</sub><sup>-</sup> electrolyte under different incident light intensities (0 Sun, 0.1 Sun, 0.3 Sun, 0.5 Sun, 0.6 Sun, 0.8 Sun, 1.0 Sun).

Despite the advantages in *V*<sub>oc</sub> and FF, DSSCs based on DOBT-IV~VI with Co(II)/(III) electrolyte have much lower PCE than their counterparts with I<sup>-</sup>/I<sub>3</sub><sup>-</sup> electrolyte due to the considerably low *J*<sub>sc</sub>. Since we employed much thicker TiO<sub>2</sub> films for devices with I<sup>-</sup>/I<sub>3</sub><sup>-</sup> electrolyte, it's not surprise to see this result. However, what we are really concerned about is whether the larger size, heavier mass and slower diffusion of cobalt complexes pose a problem in their mass transport. So the measurement of photocurrent density behaviour with dependence of incident light intensity was employed to examine if the mass transport limitation happened in our DSSCs systems. The I-V curves of DOBT-IV~VI-based DSSCs with Co(II)/(III) and I<sup>-</sup>/I<sub>3</sub><sup>-</sup> electrolyte under different incident light intensities was measured and showed in Fig. 4. In addition, the behaviours of other parameters such as open current voltage (*V*<sub>oc</sub>), fill factor (FF) and photoelectric conversion efficiency (PCE) to give

a whole view of how the performance varies with the incident light intensity (see Fig. 5).



**Fig. 5.** Behaviors of performance parameters with dependence of incident light intensity of **DOBT-IV~VI**-based DSSCs with Co(II)/(III) and  $I^-/I_3^-$  electrolyte.

According to Prof. Grätzel, a linear increase in  $J_{sc}$  with the light intensity can indicate no mass transport problems in the system.<sup>28</sup> From the photocurrent behaviour, we can find that both photocurrents of DSSCs with Co(II)/(III) and  $I^-/I_3^-$  electrolyte are in direct ratio with the incident light density ( $I_1$ ). The similar trends of their photocurrent behaviour with the incident light density indicate that the impact of mass transport limitation of Co(II)/(III) redox couples doesn't seem to be a problem in our system. In addition, for DSSCs with  $I^-/I_3^-$  electrolyte, the  $J_{sc}$  of **DOBT-V**-based DSSCs are much higher than that of **DOBT-IV**- and **DOBT-VI**-based DSSCs, between which there is nearly no difference. On the other hand, for DSSCs with Co(II)/(III) electrolyte, the  $J_{sc}$  decreases in the order of  $J_{sc}(\text{DOBT-V}) > J_{sc}(\text{DOBT-VI}) > J_{sc}(\text{DOBT-IV})$ .

As for the photovoltage behaviour, in general, the photovoltage rises slowly with the light intensity. Owing to the benefit of the more positive redox potential of cobalt complexes, high open current voltages were obtained. At the illumination intensity of 1 Sun, the  $V_{oc}$  values of 0.774, 0.760, and 0.713 V for **DOBT-IV~VI**-based DSSC, respectively, were obtained, compared to the corresponding 0.686, 0.662 and 0.629V for **DOBT-IV~VI**-based DSSC with  $I^-/I_3^-$  electrolyte, respectively. It is notable that the gaps between photovoltages of DSSCs with Co(II)/(III) electrolyte and their counterparts with  $I^-/I_3^-$  electrolyte are bigger than 0.1V, which is surprising because our sensitizers don't have blocking groups like alkyl chains on the donor moiety but still perform well with the Co(II)/(III) electrolyte. That means the alkyl chains on the auxiliary acceptors could also retard the charge recombination to some extent, but not enough. The charge recombination in DSSCs with Co(II)/(III) electrolyte is still much more severe than that in  $I^-/I_3^-$  electrolyte, which can be proved not only by electrochemical impedance spectroscopy (EIS) but also by intensity-modulated photocurrent spectroscopy (IMVS), which will be discussed in the following sections.

As for FF, there are different changing patterns between DSSCs with Co(II)/(III) and those with  $I^-/I_3^-$  electrolyte. For DSSCs with  $I^-/I_3^-$  electrolyte, their FF values decrease with the incident light intensity are close to each other, while FF values of DSSCs with Co(II)/(III) electrolyte soared at the range of 0.1 Sun to 0.3 Sun, then gradually decline with the increasing light intensity and show in the order of FF (**DOBT-IV**) > FF (**DOBT-V**) > FF (**DOBT-IV**). We are

not clear about the reason for this yet. Despite all those, the overall photoelectric conversion efficiencies at different light intensities vary in a similar way, which climb up and down twice, with peaks at the incident light intensities of 0.3162 Sun and 0.7943 Sun. All of them exhibit the same order of PCE (**DOBT-V**) > PCE (**DOBT-IV**) > PCE (**DOBT-VI**).

### Electrochemical Impedance Spectroscopy (EIS)

The electrochemical impedance spectroscopy (EIS) was employed to help us understand the differences of  $V_{oc}$ . Typical Nyquist and Bode plots can be found in Fig. 6, which were obtained by applying -0.70 V bias in the dark at the frequency range from 0.1 Hz to 100 Hz.  $R_s$ ,  $R_{CE}$  and  $R_{res}$ , which represent the series impedance, the charge transfer impedances at the interface of Pt/electrolyte and the interface of  $TiO_2$ /dye/electrolyte, are in accordance with the intercept on the horizontal axis, the radiuses of the first and second semicircles in the Nyquist plot, respectively. Generally speaking, the large  $R_{res}$  will retard the charge recombination at the interface of  $TiO_2$ /dye/electrolyte, leading to the increasing electron concentration in the semiconductor, thus results in the rise of the Fermi energy level of  $TiO_2$ , which will enhance the  $V_{oc}$ . It is easy to understand the high  $V_{oc}$  of **DOBT-IV**-based DSSC since it has the largest  $R_{res}$ , no matter with which kind of electrolytes.

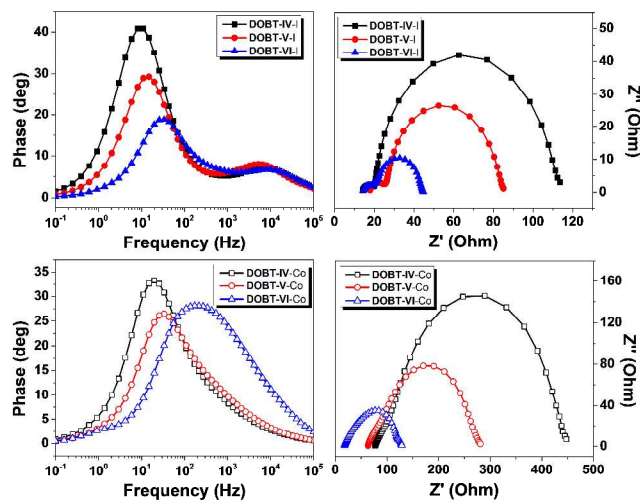


**Fig. 6.** The Nyquist plots Bode plots of **DOBT-IV~VI**-based DSSCs with  $I^-/I_3^-$  and Co(II)/(III) electrolyte, which were all measured applying bias of 0.70 V in the dark.

The electron lifetimes were calculated according to the Bode plots through the equation of  $\tau_e = 1/(2\pi f)$ , in which  $f$  represents the frequency of the highest peak. With the Co(II)/(III) electrolyte, the electron lifetimes for **DOBT-IV~VI**-based DSSCs are 8.06 ms, 5.13 ms, 0.82 ms, respectively. In contrast, the electron lifetimes for **DOBT-IV~VI**-based DSSCs with  $I^-/I_3^-$  electrolyte are much higher, reaching 16.58 ms, 11.70 ms and 5.35 ms, respectively. The simulated results obtained by using equivalent circuit of R(QR)(QR) for DSSCs with  $I^-/I_3^-$  and Co(II)/(III) electrolyte can be found in Table S3.

Suggested by Juan Bisquert, the electron lifetime  $\tau_n$ , which representing the response time constant for recombination, is a product of a recombination resistance and a capacitance. It can be written as  $\tau_n = R_{rec}C$ , where  $C$  is the capacitance at the  $TiO_2$ /dye/electrolyte interface.<sup>29</sup> The fitted relationship between electron lifetime in DSSCs and applied biases have been displayed in Fig. 7, which was obtained from Nyquist plots measured under different biases in the dark. According to Fig. 7, the lifetime figures in **DOBT-IV**-based DSSCs are the longest in both electrolytes. On the

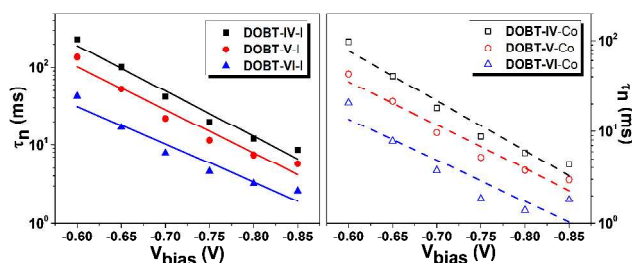


Fig. 7. The electron lifetime as a function of applied bias in **DOBT-IV-VI**-based DSSCs with  $I/I_3^-$  and  $Co(II)/(III)$  electrolyte, which were obtained by EIS under various biases in the dark.

contrary, **DOBT-VI**-based DSSCs always have the shortest electron lifetime. In addition, the electron lifetimes in DSSCs with  $I/I_3^-$  electrolyte are higher than their counterparts with  $Co(II)/(III)$  electrolyte. This strongly indicates that there are serious charge recombination problems in the  $Co(II)/(III)$  electrolyte system and **DOBT-VI**-based DSSCs.

### Intensity-Modulated Photovoltage Spectroscopy (IMVS)

Since the current in EIS is supplied by an external voltage source, we also employed intensity modulated photovoltage spectroscopy (IMVS) to further investigate the band edge movement and recombination kinetics in dye-sensitized solar cells, where the current is generated by the adsorbed dye on the  $TiO_2$  surface.<sup>30</sup>

By using a small sinusoidal perturbation of the light intensity, the periodic response of the photovoltage is measured. Since the IMVS response is determined by the electron lifetime under open circuit conditions, it gives us a reliable insight of electron recombination and changes in  $V_{oc}$ . From the Fig. 8, the DSSCs with  $Co(II)/(III)$  electrolyte have much shorter electron lifetimes than their counterparts with  $I/I_3^-$  electrolyte, further confirmed what we have analyzed in the EIS. Under the open current condition, there are larger dark currents in the DSSCs with  $Co(II)/(III)$  electrolyte, which are unfavorable and lower the Fermi level  $E_{F,n}$  in the dark. They also follow the order of  $\tau_n$  (**DOBT-IV**) >  $\tau_n$  (**DOBT-V**) >  $\tau_n$  (**DOBT-VI**), which is in accordance with their  $V_{oc}$ .

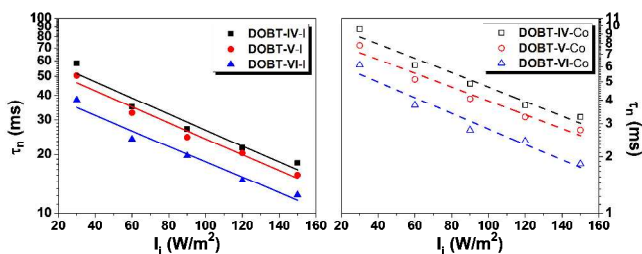


Fig. 8. The electron lifetime derived from intensity modulated photovoltage spectroscopy of **DOBT-IV-VI**-based DSSCs with  $I/I_3^-$  and  $Co(II)/(III)$  electrolyte.

Given the results of EIS and IMPS, we speculate the reason for enhanced  $V_{oc}$  due to the use of  $Co(II)/(III)$  electrolyte but shorter lifetime than devices with  $I/I_3^-$  electrolyte. It is known that  $V_{oc} = E_{F,n} - E_{redox}$ , where the  $E_{F,n}$  is the Fermi energy level of  $TiO_2$  and  $E_{redox}$  is the redox potential of the redox shuttles in the electrolyte. In comparison with  $I/I_3^-$  electrolyte, even though the  $E_{F,n}$  of the semiconductor layer in DSSCs with  $Co(II)/(III)$  electrolyte are more positive owing to the shorter electron lifetimes which indicate less electron concentrations in  $TiO_2$ , the differences between them are quite small. Considering that the  $E_{redox}$  of  $Co(II)/(III)$  redox couples (0.56 V vs. NHE) is much more positive than that of  $I/I_3^-$  electrolyte

(0.4 V vs. NHE), the gaps between  $E_{F,n}$  and  $E_{redox}$  can still be widened, resulting in the large improvement of  $V_{oc}$ .

### Conclusions

In this paper, we designed and synthesized three D-A- $\pi$ -A sensitizers (**DOBT-IV-VI**) with bis(octyloxy)benzo-[c][1,2,5]thiadiazole as the auxiliary acceptor. We used *N,N*-diphenylthiophen-2-amine as donor to enlarge the absorption range and obtain high  $J_{sc}$ . The goal was fulfilled and via fine tuning of the  $\pi$ -bridge, the highest photoelectric conversion efficiency of 7.16% was achieved with  $J_{sc} = 16.88 \text{ mAcm}^{-2}$ ,  $V_{oc} = 0.662 \text{ V}$  and FF = 64.03% for the **DOBT-V**-based DSSCs employing iodide/triiodide electrolyte. To address the problem of low  $V_{oc}$ ,  $Co(II)/(III)$  electrolyte was applied to them. The  $V_{oc}$  values were enhanced significantly, but owing to the big drop in  $J_{sc}$ , we failed to further enhance the performance and ended up in the highest PCE of 6.14% with  $J_{sc} = 11.35 \text{ mAcm}^{-2}$ ,  $V_{oc} = 0.760 \text{ V}$  and FF = 71.16% for the **DOBT-V**-based DSSCs. Density functional theory calculations were employed to explain the differences of optical properties and electrochemical properties among the three dyes induced by changing  $\pi$ -bridge. Behavior study of the four performance parameters provide a whole view of how they vary with the incident light intensity when  $Co(II)/(III)$  and  $I/I_3^-$  electrolyte are used. Furthermore, EIS and IMVS were engaged in proving that the much more severe charge recombination in DSSCs with  $Co(II)/(III)$  electrolyte than that in  $I/I_3^-$  electrolyte and the order of  $V_{oc}$  (**DOBT-IV**) >  $V_{oc}$  (**DOBT-V**) >  $V_{oc}$  (**DOBT-VI**). The results show the alkyl chains on the auxiliary acceptors could retard the charge recombination to some extent, but not enough. Therefore, further improvement could focus on the adding some blocking groups like alkyl chains on the donor moiety to enhance their performance in dye-sensitized solar cells.

### Experimental Section

#### Instruments and characterization

$^1H$  NMR and  $^{13}C$  NMR spectra were obtained via a Brücker AM 400 spectrometer. Mass spectra were measured using an ESI mass spectrometer. A Varian Cary 500 spectrophotometer was utilized to measure the UV-Vis spectra. A Versastat II electrochemical workstation (Princeton applied research) was employed to get the cyclic voltammograms of dyes with a three-electrode system, in which a Pt working electrode, a Pt wire counter electrode, and a regular calomel reference electrode in saturated KCl solution were used. The film thickness was measured using a step profiler (Veeco Dektak 150).

The photovoltaic characterization was performed on the setup that constitutes a 450 W xenon lamp (Oriel), a Schott K113 Tempax sunlight filter (PräzisionsGlas & Optik GmbH), and a source meter (Keithley 2400) which applies potential bias and measures the photogenerated current. A set of circular variable neutral density filters (Unice E-O Services Inc. in Taiwan) was used to adjust the light intensity. The incident light intensities we used were 1.0 Sun, 0.8 Sun, 0.6 Sun, 0.5 Sun, 0.3 Sun and 0.1 Sun. IPCE was obtained using a SR830 lock-in amplifier, a 300 W xenon lamp (ILC Technology) and a Gemini-180 double monochromator (Jobin-Yvon Ltd.). The electrochemical impedance spectroscopy measurements of all the DSSCs were performed using a Zahner IM6e Impedance Analyzer (ZAHNER-Elektrik GmbH & CoKG, Kronach, Germany). The frequency range is 0.1 Hz-100 kHz. The applied voltage bias is from -0.60 V to -0.85 V. The magnitude of the alternating signal is 5 mV. Intensity modulated photovoltage spectroscopy was obtained by

the Zahner IM6e Impedance Analyzer (ZAHNER-Elektrik GmbH & CoKG, Kronach, Germany) and a light-emitting display array ( $\lambda = 457$  nm, blue light). The frequency range is 0.1 Hz-100 kHz.

### Fabrication of dye-sensitized solar cells

For the DSSCs with iodine electrolyte, three layers of Dyesol 90-T TiO<sub>2</sub> paste and a scattering layer were screen-printed onto the FTO glass before sintered gradually up to 500 °C. While for the DSSCs with cobalt electrolyte, the pre-treatment of FTO glass was carried out by immersing the FTO glass into 40 mM TiCl<sub>4</sub> aqueous solution at 70 °C for 30 min three times before sintered at 450 °C for 30 min. Then one layer of Dyesol 90-T TiO<sub>2</sub> paste and a scattering layer were screen-printed onto the FTO glass and sintered gradually up to 500 °C. After the post-treatment of 40 mM TiCl<sub>4</sub> aqueous solution at 70 °C for 30 min, the photoanodes were calcinated at 450 °C for 30min and cooled down to 80 °C before a  $3 \times 10^{-4}$  M dye bath in CH<sub>3</sub>CH<sub>2</sub>OH : CHCl<sub>3</sub> = 7:3(v/v) solution. The dye bath lasted for 14 h for DSSCs with iodine electrolyte and for 6.5 h for DSSCs with cobalt electrolyte. After rinsed with ethanol, the dye-sensitized photoanodes were sealed with platinized counter electrodes using 25- $\mu$ m-thick Surlyn (Dupont) as a binder and a spacer. The electrolytes were introduced to the cells via two pre-drilled holes in the counter electrodes. The composition of the iodine electrolyte is as follows: 0.05 M I<sub>2</sub>, 0.1 M LiI, 0.5 M 1,2-dimethyl-3-propylimidazolium iodide (DMPH), 0.75 M 4-tert-butylpyridine (tBP) in acetonitrile. The composition of the cobalt electrolyte is as follows: 0.22 M tris(2,2'-bipyridine)cobalt(II) bis(hexafluorophosphate) ([Co(bpy)<sub>3</sub>](PF<sub>6</sub>)<sub>2</sub>), 0.05 M tris(2, 2'-bipyridine)cobalt(III)tris(hexafluorophosphate) ([Co(bpy)<sub>3</sub>](PF<sub>6</sub>)<sub>3</sub>), 0.1 M LiClO<sub>4</sub>, 0.2 M tBP in acetonitrile. The thicknesses of TiO<sub>2</sub> film for DSSCs with are I<sup>-</sup>/I<sub>3</sub><sup>-</sup> and Co(II)/(III) electrolyte are 8.3  $\mu$ m and 4.8  $\mu$ m, respectively. The active area of all DSSCs is 0.25 cm<sup>2</sup>.

### Materials and reagents

Fluorine-doped SnO<sub>2</sub> conducting glass (FTO glass, transparency > 90%, sheet resistance 15  $\Omega/\square$ ) was obtained from the Geao Science and Educational Co. Ltd. of China. Acetonitrile, Tetra-n-butyl ammonium hexafluorophosphate (TBAPF<sub>6</sub>), 4-tert-butylpyridine, and lithium iodide were bought from Fluka and iodine (99.999%) was purchased from Alfa Aesar. All chemicals and reagents were purchased from suppliers and used without further purification. Tetrahydrofuran (THF) was dried with sodium before use.

### Synthesis

**N, N-diphenyl-5-(tributylstannyl)thiophen-2-amine (2).** N, N-diphenylthiophen-2-amine (2.51 g, 10 mmol) was dissolved 10mL anhydrous tetrahydrofuran (THF). The solution was cooled down to -78 °C under argon. 1.6 M n-butyllithium in n-hexane (7.5 mL, 12 mM) was added dropwise and stirred for 1 h. After the reaction at room temperature for 30 min, the mixture was cooled to -78 °C and stirred for another 30 min. Tributyltin chloride was injected fast into the mixture and stirred for 2 h at -78 °C, followed by another 2 h at room temperature. Then salt water was added to quench the reaction. The crude product was extracted by CH<sub>2</sub>Cl<sub>2</sub> and dried by anhydrous MgSO<sub>4</sub>. Then 20 mL dimethylformamide (DMF) was added to produce 0.5 mM/ml brown solution.

**5-(7-bromo-5,6-bis(octyloxy)benzo[c][1,2,5]thiadiazol-4-yl)-N,N-diphenylthiophen-2-amine (3).** A mixture of 4,7-dibromo-5,6-bis(octyloxy)benzo[c][1,2,5]thiadiazole (275 mg, 0.5 mM) and tetrakis(triphenylphosphine)palladium (Pd(PPh<sub>3</sub>)<sub>4</sub>) (20 mg, 0.018 mM) in 20 mL dimethylformamide (DMF) was heated and refluxed

under argon for 15min. After the compound **2** in DMF (270 mg, 0.5 mM) was added, the mixture was refluxed for 20 h before cooled down to room temperature, when the solution was red. The mixture was poured into salt water and stirred to precipitate the crude product, which was filtered and washed with salt water, followed by extraction using CH<sub>2</sub>Cl<sub>2</sub> and water. The combined organic phase was dried by anhydrous MgSO<sub>4</sub> and the solvent was removed under reduce pressure. The crude product was purified by chromatography with petroleum ether (PE)/CH<sub>2</sub>Cl<sub>2</sub> (5:1, v/v) as the eluent to get 145 mg red solid. Yield: 40%. <sup>1</sup>H NMR (400 MHz, CDCl<sub>3</sub>):  $\delta$  8.25 (d,  $J = 4$  Hz, 1H), 7.20-7.25 (m, 4H), 7.16-7.19 (m, 2H), 6.98-7.03 (m, 2H), 4.06 (q,  $J = 6.8$  Hz, 2H), 3.97 (q,  $J = 7.2$  Hz, 2H), 1.77-1.87 (m, 2H), 1.65-1.74 (m, 2H), 1.18-1.31 (m, 20H), 0.80-0.84 (m, 6H).

**4-(7-(5-(diphenylamino)thiophen-2-yl)-5,6-bis(octyloxy)benzo[c][1,2,5]thiadiazol-4-yl)benzaldehyde (4).** 2 M K<sub>2</sub>CO<sub>3</sub> (aq., 5 mL), Pd(PPh<sub>3</sub>)<sub>4</sub> (20 mg, 0.018 mM) and compound **3** (240 mg, 0.4 mM) in 20 mL THF was heated and refluxed for 15 min under argon before the solution (4-formylphenyl)boronic acid (75 mg, 0.5 mM) in THF was added. After refluxed for 20 h, the mixture was cooled down to room temperature and the solvent was evaporated. After being extracted with CH<sub>2</sub>Cl<sub>2</sub> and water, the organic layers were combined and dried by anhydrous MgSO<sub>4</sub>. The solvent was removed under reduce pressure. The residue was purified by chromatography with PE/CH<sub>2</sub>Cl<sub>2</sub> (1:1, v/v) as the eluent to get 200 mg red solid. Yield: 67%. <sup>1</sup>H NMR (400 MHz, CDCl<sub>3</sub>):  $\delta$  10.10 (s, 1H), 8.41 (d,  $J = 4.4$  Hz, 1H), 8.02 (d,  $J = 8.4$  Hz, 2H), 7.91 (d,  $J = 8$  Hz, 1H), 7.25-7.33 (m, 8H), 7.06-7.11 (m, 2H), 6.75 (d,  $J = 4$  Hz, 2H), 4.12 (q,  $J = 6.8$  Hz, 2H), 3.82 (q,  $J = 6.8$  Hz, 2H), 1.77-1.85 (m, 2H), 1.46-1.53 (m, 2H), 1.25-1.34 (m, 20H), 0.84-0.91 (m, 6H).

**5-(7-(5-(diphenylamino)thiophen-2-yl)-5,6-bis(octyloxy)benzo[c][1,2,5]thiadiazol-4-yl)furan-2-carbaldehyde (5).** Compound **5** was synthesized in a similar way to compound **4** by replacing (4-formylphenyl)boronic acid with (5-formylfuran-2-yl)boronic acid. The residue was purified by chromatography with PE/CH<sub>2</sub>Cl<sub>2</sub> (1:1, v/v) as the eluent to get 224 mg purplish red solid. Yield: 70%. <sup>1</sup>H NMR (400 MHz, CDCl<sub>3</sub>):  $\delta$  9.76 (s, 1H), 8.48 (d,  $J = 4$  Hz, 1H), 7.63 (d,  $J = 4$  Hz, 1H), 7.44 (d,  $J = 4$  Hz, 1H), 7.27-7.34 (m, 8H), 7.10 (q,  $J = 7.2$  Hz, 2H), 6.73 (d,  $J = 4.4$  Hz, 1H), 4.06-4.15 (m, 4H), 1.88-1.96 (m, 2H), 1.76-1.84 (m, 2H), 1.23-1.38 (m, 20H), 0.86-0.91 (m, 6H).

**5-(7-(5-(diphenylamino)thiophen-2-yl)-5,6-bis(octyloxy)benzo[c][1,2,5]thiadiazol-4-yl)thiophene-2-carbaldehyde (6).** Compound **6** was synthesized in a similar way to compound **4** by replacing (4-formylphenyl)boronic acid with (5-formylthiophen-2-yl)boronic acid. The residue was purified by chromatography with PE/CH<sub>2</sub>Cl<sub>2</sub> (1:1, v/v) as the eluent to get 160 mg purplish red solid. Yield: 53%. <sup>1</sup>H NMR (400 MHz, CDCl<sub>3</sub>):  $\delta$  10.00 (s, 1H), 8.66 (d,  $J = 4$  Hz, 1H), 8.44 (d,  $J = 4.4$  Hz, 1H), 7.85 (d,  $J = 4$  Hz, 1H), 7.27-7.34 (m, 8H), 7.10 (q,  $J = 7.2$  Hz, 2H), 6.74 (d,  $J = 4.4$  Hz, 1H), 4.14 (q,  $J = 7.2$  Hz, 2H), 4.06 (q,  $J = 7.2$  Hz, 2H), 1.87-1.95 (m, 2H), 1.77-1.85 (m, 2H), 1.25-1.43 (m, 20H), 0.86-0.91 (m, 6H).

**(E)-2-cyano-3-(4-(7-(5-(diphenylamino)thiophen-2-yl)-5,6-bis(octyloxy)benzo[c][1,2,5]thiadiazol-4-yl)phenyl)acrylic acid (DOBT-IV).** A mixture of compound **4** (128 mg, 0.17 mM), cyanoacetic acid (102 mg, 1.2 mM) ammonium acetate (120 mg) and acetic acid (14 mL) was refluxed under argon for 20 h before cooled down to room temperature. Then the mixture was poured into salt water to precipitate the crude product before the extraction using CH<sub>2</sub>Cl<sub>2</sub> and water. The combined organic phase was dried by anhydrous MgSO<sub>4</sub> and the solvent was removed under reduce

pressure. The crude product was purified by chromatography with  $\text{CH}_2\text{Cl}_2/\text{CH}_3\text{CH}_2\text{OH}$  (100:6, v/v) as the eluent to get 114.6 mg dark red solid. Yield: 83%.  $^1\text{H}$  NMR (400 MHz,  $\text{DMSO-d}_6$ ):  $\delta$  8.38 (s, 1H), 8.24 (s, 1H), 8.09 (d,  $J = 3.6$  Hz, 1H), 7.80-7.77 (m, 2H), 7.34-7.41 (m, 4H), 7.19 (d,  $J = 7.2$  Hz, 4H), 7.14-7.11 (m, 2H), 6.73-6.69 (m, 1H), 4.04 (m,  $J = 4.4$  Hz, 2H), 3.77 (m,  $J = 4.4$  Hz, 2H), 1.69 (d,  $J = 3.2$  Hz, 2H), 1.43-1.41 (m, 2H), 1.32-1.21 (m, 20H), 0.78-0.85 (m, 6 H).  $^{13}\text{C}$  NMR (100 MHz,  $\text{DMSO-d}_6$ ), 163.4, 153.7, 152.9, 151.4, 151.1, 149.6, 149.5, 146.9, 137.2, 131.4, 130.5, 129.6, 129.5, 124.9, 123.9, 123.3, 123.1, 122.4, 121.5, 117.8, 117.2, 116.9, 114.5, 74.0, 73.7, 31.2, 31.1, 29.6, 29.4, 29.0, 28.8, 28.6, 28.5, 25.4, 25.3, 22.0, 13.9. HRMS (ESI):  $m/z$  calcd. for  $\text{C}_{48}\text{H}_{52}\text{N}_4\text{O}_4\text{S}_2$ : 811.3352; found 811.3349.

**(Z)-2-cyano-3-(5-(7-(5-(diphenylamino)thiophen-2-yl)-5,6-bis(octyloxy)benzo[c][1,2,5]thiadiazol-4-yl)furan-2-yl)acrylic acid (DOBT-V).** DOBT-V was synthesized in a similar way to DOBT-IV by compound 4 with compound 5. The residue was purified by chromatography with  $\text{CH}_2\text{Cl}_2/\text{CH}_3\text{CH}_2\text{OH}$  (100:6, v/v) as the eluent to get 175 mg deep dark red solid. Yield: 78%.  $^1\text{H}$  NMR (400 MHz,  $\text{DMSO-d}_6$ ):  $\delta$  8.44 (d,  $J = 4.4$  Hz, 1H), 7.98 (s, 1H), 7.61 (d,  $J = 3.6$  Hz, 1H), 7.50 (d,  $J = 3.6$  Hz, 1H), 7.38 (q,  $J = 7.2$  Hz, 4H), 7.21 (d,  $J = 7.2$  Hz, 4H), 7.15 (q,  $J = 7.2$  Hz, 2H), 6.69 (d,  $J = 4$  Hz, 1H), 3.98-4.04 (m,  $J = 7.2$  Hz, 2H), 1.68-1.75 (m, 4H), 1.22-1.36 (m, 20H), 0.81-0.87 (m, 6H).  $^{13}\text{C}$  NMR (100 MHz,  $\text{DMSO-d}_6$ ), 175.7, 175.1, 163.8, 160.1, 159.6, 156.0, 153.7, 152.4, 150.7, 148.7, 148.0, 146.5, 132.4, 132.2, 132.1, 131.1, 130.4, 130.0, 129.7, 125.1, 124.0, 120.1, 114.3, 114.1, 67.5, 31.2, 29.0, 28.7, 28.6, 25.5, 22.1, 13.9. HRMS (ESI):  $m/z$  calcd. for  $\text{C}_{46}\text{H}_{50}\text{N}_4\text{O}_5\text{S}_2$ : 801.3144; found 801.3146.

**(Z)-2-cyano-3-(5-(7-(5-(diphenylamino)thiophen-2-yl)-5,6-bis(octyloxy)benzo[c][1,2,5]thiadiazol-4-yl)thiophen-2-yl)acrylic acid (DOBT-VI).** DOBT-VI was synthesized in a similar way to DOBT-IV by compound 4 with compound 6. The residue was purified by chromatography with  $\text{CH}_2\text{Cl}_2/\text{CH}_3\text{OH}$  (100:8, v/v) as the eluent to get 71.5 mg deep dark red solid. Yield: 72%.  $^1\text{H}$  NMR (400 MHz,  $\text{DMSO-d}_6$ ):  $\delta$  10.75 (s, 1 H), 8.60 (s, 1 H), 8.46 (s, 1 H), 7.60 (s, 1 H), 7.40 (s, 2 H), 7.11-7.16 (m, 4 H), 7.00 (d,  $J = 7.6$  Hz, 4H), 6.90-6.93 (m, 4 H), 4.07 (s, 2 H), 3.66 (s, 2 H), 1.98 (s, 2 H), 1.14-1.27 (m, 22 H), 0.74 (m, 6 H).  $^{13}\text{C}$  NMR (100 MHz,  $\text{DMSO-d}_6$ ), 152.7, 152.6, 150.1, 147.6, 137.7, 131.9, 129.2, 126.9, 124.6, 123.1, 121.9, 116.2, 74.2, 74.1, 31.9, 30.1, 30.0, 29.7, 29.5, 29.4, 29.3, 26.1, 26.0, 22.6, 13.6, 13.5. HRMS (ESI):  $m/z$  calcd. for  $\text{C}_{46}\text{H}_{50}\text{N}_4\text{O}_4\text{S}_3$ : 817.2916; found 817.2914.

## Acknowledgements

This work was supported by NSFC/China (2116110444, 21172073, 91233207 and 21372082) and the National Basic Research 973 Program (2013CB733700).

## Notes and references

<sup>a</sup> Key Laboratory for Advanced Materials and Institute of Fine Chemicals East China University of Science and Technology Shanghai 200237, China  
Fax: +86-21-64252758  
E-mail: jlhua@ecust.edu.cn;  
<sup>b</sup>Department of Theoretical Chemistry and Biology, School of Biotechnology, KTH Royal Institute of Technology Stockholm 10691, Sweden  
Electronic Supplementary Information (ESI) available: [cyclic voltammetry, molecular orbital calculation results, the simulated parameters from EIS]. See DOI: 10.1039/b000000x/

- B. O'Regan and M. Grätzel, *Nature*, 1991, **343**, 737.
- J. Burschka, N. Pellet, S. J. Moon, R. Humphry-Baker, P. Gao, M. K. Nazeeruddin and M. Grätzel, *Nature*, 2013, **499**, 316; M. Liu, M. B. Johnston and H. J. Snaith, *Nature*, 2013, **501**, 395.
- S. Mathew, A. Yella, P. Gao, R. Humphry-Baker, B. F. E. Curchod, N. Ashari-Astani, I. Tavernelli, U. Rothlisberger, M. K. Nazeeruddin, and M. Grätzel, *Nature Chemistry*, 2014, **6**, 242.
- A. Yella, H. W. Lee, H. N. Tsao, C. Y. Yi, A. K. Chandiran, M. K. Nazeeruddin, E. W. G. Diau, C. Y. Yeh, S. M. Zakeeruddin and M. Grätzel, *Science*, 2011, **334**, 629; C. M. Lan, H. P. Wu, T. Y. Pan, C. W. Chang, W. S. Chao, C. T. Chen, C. L. Wang, C. Y. Lin and E. W. G. Diau, *Energy Environ. Sci.*, 2012, **5**, 6460; A. K. Chandiran, N. Tetreault, R. Humphry-Baker, F. Kessler, E. Baranoff, C. Y. Yi, M. K. Nazeeruddin and M. Grätzel, *Nano Lett.*, 2012, **12**, 3941; J. H. Yum, E. Baranoff, S. Wenger, M. K. Nazeeruddin and M. Grätzel, *Energy Environ. Sci.*, 2011, **4**, 842; L. Y. Han, A. Islam, H. Chen, C. Malapaka, B. Chiranjeevi, S. F. Zhang, X. D. Yang and M. Yanagida, *Energy Environ. Sci.*, 2012, **5**, 6057.
- S. M. Feldt, E. A. Gibson, E. Gabriellsson, L. Sun, G. Boschloo and A. Hagfeldt, *J. Am. Chem. Soc.*, 2010, **132**, 16714; J. H. Yum, E. Baranoff, F. Kessler, T. Moehl, S. Ahmad, T. Bessho, A. Marchioro, E. Ghadiri, J. E. Moser, C. Y. Yi, M. K. Nazeeruddin, and M. Grätzel, *Nature Communications*, 2012, **3**, 2041; P. Salvatori, G. Marotta, A. Cinti, E. Mosconi, M. Panigrahi, L. Giribabu, M. K. Nazeeruddin, F. De Angelis, *Inorganica Chimica Acta*, 2013, **406**, 106; K. B. Ariiba, T. Moehl, S. M. Zakeeruddin and M. Grätzel, *Chemical Science*, 2013, **4**, 454.
- M. Liberatore, A. Petrocco, F. Caprioli, C. La Mesa, F. Decker and C. A. Bignozzi, *Electrochim. Acta*, 2010, **55**, 4025; X. P. Zong, M. Liang, C. R. Fan, K. Tang, G. Li, Z. Sun and S. Xue, *J. Phys. Chem. C*, 2012, **116**, 11241; C. J. Qin, W. Q. Peng, K. Zhang, A. Islam and L. Y. Han, *Organic Letters*, 2012, **14**, 2532; P. Gao, Y. J. Kim, J. H. Yum, T. W. Holcombe, M. K. Nazeeruddin and M. Grätzel, *J. Mater. Chem. A*, 2013, **1**, 5535; AN. Cai, Y. L. Wang, M. F. Xu, Y. Fan, R. Z. Li, M. Zhang and P. Wang, *Adv. Funct. Mater.*, 2013, **23**, 1846.
- J. Liu, X. D. Yang, A. Islam, Y. Numata, S. F. Zhang, N. T. Salim, J. Chen and L. Y. Han, *J. Mater. Chem. A*, 2013, **1**, 10889; X. D. Yang, S. F. Zhang, K. Zhang, J. Liu, C. J. Qin, H. Chen, A. Islam and L. Y. Han, *Energy Environ. Sci.*, 2013, **6**, 3637; J. Liu, Y. Numata, C. J. Qin, A. Islam, X. D. Yang and L. Y. Han, *Chem. Commun.*, 2013, **49**, 7587; Y. Bai, J. Zhang, D. F. Zhou, Y. H. Wang, M. Zhang and P. Wang, *J. Am. Chem. Soc.*, 2011, **133**, 11442; X. F. Lu, Q. Y. Feng, T. Lan, G. Zhou and Z. S. Wang, *Chem. Mater.*, 2012, **24**, 3179.
- Y. P. Hong, J. Y. Liao, D. R. Cao, X. F. Zang, D. B. Kuang, L. Y. Wang, H. Meier and C. Y. Su, *J. Org. Chem.*, 2011, **76**, 8015; Y. Hao, X. C. Yang, M. Z. Zhou, J. Y. Cong, X. N. Wang, A. Hagfeldt and L. C. Sun, *ChemSusChem*, 2011, **4**, 1601; Y. Ooyama, Y. Shimada, S. Inoue, T. Nagano, Y. Fujikawa, K. Komaguchi, I. Imae and Y. Harima, *New J. Chem.* 2011, **35**, 111; S. Haid, M. Marszalek, A. Mishra, M. Wielopolski, J. Teuscher, J.-E. Moser, R. Humphry-Baker, S. M. Zakeeruddin, M. Grätzel and P. Bäuerle, *Adv. Funct. Mater.*, 2012, **22**, 1291; N. Cai, Y. L. Wang, M. F. Xu, Y. Fan, R. Z. Li, M. Zhang and P. Wang, *Adv. Funct. Mater.*, 2013, **23**, 1846.
- Y. Z. Wu and W. H. Zhu, *Chem. Soc. Rev.*, 2013, **42**, 2039.
- M. Velusamy, K. R. Justin Thomas, J. T. Lin, Y. C. Hsu and K. C. Ho, *Org. Lett.*, 2005, **7**, 1899; W. H. Zhu, Y. Z. Wu, S. T. Wang, W. Q. Li, X. Li, J. Chen, Z. S. Wang and H. Tian, *Adv. Funct. Mater.*, 2011, **21**, 756; Y. Z. Wu, X. Zhang, W. Q. Li, Z. S. Wang, H. Tian and W. H. Zhu, *Adv. Energy Mater.*, 2012, **2**, 149; M. Zhang, Y. L. Wang, M. F. Xu, W. T. Ma, R. Z. Li and P. Wang, *Energy Environ. Sci.*, 2013, **6**, 2944.
- Y. Cui, Y. Z. Wu, X. F. Lu, X. Zhang, G. Zhou, F. B. Miapah, W. H. Zhu and Z. S. Wang, *Chem. Mater.*, 2011, **23**, 4394; J. Y. Mao, F. L. Guo, W. J. Ying, W. J. Wu, J. Li and J. L. Hua, *Chem.-Asian J.*, 2012, **7**, 982.
- D. W. Chang, H. J. Lee, J. H. Kim, S. Y. Park, S. M. Park, L. Dai and J. B. Baek, *Org. Lett.*, 2011, **13**, 3880; K. Pei, Y. Z. Wu, W. J. Wu, Q. Zhang, B. Q. Chen, H. Tian and W. H. Zhu, *Chem.-Eur. J.*, 2012, **18**, 8190; X. F. Lu, Q. Y. Feng, T. Lan, G. Zhou and Z. S. Wang, *Chem. Mater.*, 2012, **24**, 3179; K. Pei, Y. Z. Wu, A. Islam, Q. Zhang, L. Y. Han, H. Tian and W. H. Zhu, *ACS Appl. Mater. Interfaces*, 2013, **5**, 4986.

- 13 S. Y. Qu, W. J. Wu, J. L. Hua, C. Kong, Y. T. Long and H. Tian, *J. Phys. Chem. C*, 2010, **114**, 1343; S. Y. Qu, B. Wang, F. L. Guo, J. Li, W. J. Wu, C. Kong, Y. T. Long and J. L. Hua, *Dyes and Pigments*, 2012, **92**, 1384; S. Y. Qu, C. J. Qin, A. Islam, Y. Z. Wu, W. H. Zhu, J. L. Hua, H. Tian and L. Y. Han, *Chem. Commun.*, 2012, **48**, 6972; J. H. Yum, T. W. Holcombe, Y. J. Kim, K. Rakstys, T. Moehl, J. Teuscher, J. H. Delcamp, M. K. Nazeeruddin and M. Grätzel, *Scientific Reports*, 2013, **3**, 2446.
- 14 W. J. Ying, J. B. Yang, M. Wielopolski, T. Moehl, J. E. Moser, P. Comte, J. L. Hua, S. M. Zakeeruddin, H. Tian and M. Grätzel, *Chem. Sci.*, 2014, **5**, 206.
- 15 Q. Y. Feng, X. F. Lu, G. Zhou and Z. S. Wang, *Phys. Chem. Chem. Phys.*, 2012, **14**, 7993; Q. Y. Feng, W. Y. Zhang, G. Zhou and Z. S. Wang, *Chem. Asian J.*, 2013, **8**, 168.
- 16 M. Velusamy, K. R. J. Thomas, J. T. Lin, Y. C. Hsu and K. C. Ho, *Org. Lett.*, 2005, **7**, 1899; J. J. Kim, H. Choi, J. W. Lee, M. S. Kang, K. Song, S. O. Kang and J. Ko, *J. Mater. Chem.*, 2008, **18**, 5223.
- 17 W. H. Zhu, Y. Z. Wu, S. T. Wang, W. Q. Li, X. Li, J. Chen, Z. S. Wang and H. Tian, *Adv. Funct. Mater.*, 2011, **21**, 756; Y. Z. Wu, M. Marszalek, S. M. Zakeeruddin, Q. Zhang, H. Tian, M. Grätzel and W. H. Zhu, *Energy Environ. Sci.*, 2012, **5**, 8261; Y. Wu, X. Zhang, W. Li, Z. S. Wang, H. Tian and W. H. Zhu, *Adv. Energy Mater.*, 2012, **2**, 149.
- 18 L. Chen, X. Li, W. J. Ying, X. Y. Zhang, F. L. Guo, J. Li and J. L. Hua, *Eur. J. Org. Chem.*, 2013, **9**, 1770.
- 19 L. Y. Lin, C. H. Tsai, F. Lin, T. W. Huang, S. H. Chou, C. C. Wu and K. T. Wong, *Tetrahedron*, 2012, **68**, 7509; Y. C. Chen, H. H. Chou, M. C. Tsai, S. Y. Chen, J. T. Lin, C. F. Yao and K. Chen, *Chem. Eur. J.*, 2012, **18**, 5430; L. Y. Lin, C. H. Tsai, K. T. Wong, T. W. Huang, C. C. Wu, S. H. Chou, F. Lin, S. H. Chen and A. I. Tsai, *J. Mater. Chem.*, 2011, **21**, 5950; S. W. Chiu, L. Y. Lin, H. W. Lin, Y. H. Chen, Z. Y. Huang, Y. T. Lin, F. Lin, Y. H. Liu and K. T. Wong, *Chem. Commun.*, 2012, **48**, 1857.
- 20 M. Liang and J. Chen, *Chem. Soc. Rev.*, 2013, **42**, 3453.
- 21 J. Preat, C. Michaux, J. M. André and E. A. Perpète, *Int. J. Quantum Chem.*, 2012, **112**, 2072.
- 22 M. J. Frisch, G. W. Trucks, H. B. Schlegel, G. E. Scuseria, M. A. Robb, J. R. Cheeseman, G. Scalmani, V. Barone, B. Mennucci, G. A. Petersson, et al. Gaussian 09, Revision A.2, Gaussian, Inc.: Wallingford CT, 2009.
- 23 A. D. Becke, *J. Chem. Phys.*, 1993, **98**, 5648.
- 24 W. J. Hehre, R. Ditchfield, J. A. Pople, *J. Chem. Phys.*, 1972, **56**, 2257.
- 25 A. D. Becke, *J. Chem. Phys.*, 1996, **104**, 1040.
- 26 J. Tomasi, B. Mennucci, R. Cammi, *Chem. Rev.*, 2005, **105**, 2999.
- 27 J. X. He, F. L. Guo, X. Li, W. J. Wu, J. B. Yang and J. L. Hua, *Chem. Eur. J.*, 2012, **18**, 7903.
- 28 H. N. Tsao, P. Comte, C. Y. Yi and M. Grätzel, *Chemphyschem*, 2012, **13**, 2976.
- 29 J. Bisquert, F. Fabregat-Santiago, I. Mora-Seró, G. Garcia-Belmonte and Sixto Giménez, *J. Phys. Chem. C*, 2009, **113**, 17278.
- 30 G. Schlichthörl, S. Y. Huang, J. Sprague, A. J. Frank, *J. Phys. Chem. B*, 1997, **101**, 8141; J. Krüger, R. Plass, M. Grätzel, P. J. Cameron and L. M. Peter, *J. Phys. Chem. B*, 2003, **107**, 7536; J. van de Lagemaat, N. G. Park and A. J. Frank, *J. Phys. Chem. B*, 2000, **104**, 2044.